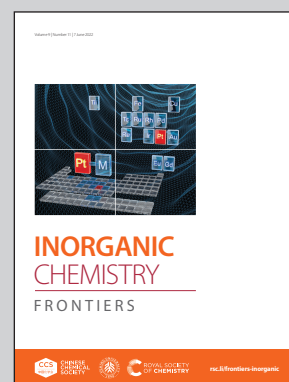


Showcasing research from Professor Manuel Ocaña's laboratory, Instituto de Ciencia de Materiales de Sevilla (ICMS), CSIC-Universidad de Sevilla, Andalucía, Spain.

Highly uniform $\text{Y}_3\text{Al}_2\text{Ga}_3\text{O}_{12}$ -based nanophosphors for persistent luminescence bioimaging in the visible and NIR regions

$\text{Y}_3\text{Al}_2\text{Ga}_3\text{O}_{12}$ doped with Ce, Cr, and Nd is one of the most interesting phosphors with persistent visible and NIR emissions. This paper describes a synthesis method to fabricate perfectly spherical and uniform nanoparticles of this material. The nanospheres form very stable colloids, present persistent luminescence, and absence of cytotoxicity, which make them ideal candidates as luminescent probes for bioimaging. Likewise, the possibility of manufacturing garnet-based nanoparticles opens the door to the development of new applications that require nanoparticulated luminescent materials, such as devices for data storage or anti-counterfeiting technology.

As featured in:



See Ana I. Becerro *et al.*, *Inorg. Chem. Front.*, 2022, **9**, 2454.

Registered charity number: 207890

RESEARCH ARTICLE

View Article Online

View Journal | View Issue

Cite this: *Inorg. Chem. Front.*, 2022, **9**, 2454Highly uniform $\text{Y}_3\text{Al}_2\text{Ga}_3\text{O}_{12}$ -based nanophosphors for persistent luminescence bioimaging in the visible and NIR regions†Encarnación Arroyo,^a Beatriz Torres Herrero,^b Jesús M. de la Fuente,^b Manuel Ocaña^a and Ana I. Becerro^a*

In the last few years, persistent phosphors with a garnet crystal structure have attracted a great deal of interest for a plethora of applications ranging from bioimaging to anti-counterfeiting technologies. However, the development of synthesis methods to fabricate uniform garnet-based micro and nanoparticles, that are needed for such applications, is not mature at all. This study reports the synthesis of highly uniform yttrium aluminum gallium garnet nanospheres. The method is based on homogeneous precipitation in a polyol medium followed by silica coating and calcination. The nanoparticles resulting after silica removal were also uniform and were easily functionalized with polyacrylic acid. The colloidal stability of the latter in physiological media and their biocompatibility were analyzed. The luminescence of the particles, doped with Ce^{3+} , Cr^{3+} , and Nd^{3+} , was studied by recording emission and excitation spectra and persistent luminescence decay curves. Due to their uniform morphology, high colloidal stability, absence of toxicity, and persistent emission in the visible and near-infrared regions, the reported nanospheres show great potential as persistent luminescent bioimaging probes. In addition, the synthesis method paves the way for future use of this persistent material in other applications that require the phosphor to be in the form of highly uniform nanoparticles.

Received 2nd March 2022,

Accepted 20th April 2022

DOI: 10.1039/d2qi00480a

rsc.li/frontiers-inorganic

1. Introduction

Persistent luminescence (PL) phosphors are materials showing continuous luminescence, from several minutes to hours, after the stoppage of the excitation with ultraviolet (UV) light, visible light, or X-rays. PL phosphors are used in very different applications, ranging from toys and security signaling to anti-counterfeiting, LED technology, and bioimaging.^{1,2} PL phosphors are especially interesting for bioimaging applications since they are charged before injection into biological tissues, thus preventing tissues autofluorescence and resulting in a higher signal to noise ratio of the bioimage.³ In addition, removal of external UV or X-rays illumination avoids the damage to living tissues. This optical bioimage approach motivated, since the beginning of the last decade, considerable development of persistent phosphors based on $\text{ZnGa}_2\text{O}_4:\text{Cr}^{3+}$,

with emission in the deep-red region centered at 695 nm.^{4–7} Such emission wavelength is inside the first biological window (650–950 nm), where absorption and scattering from blood and water in organisms are reduced and light penetration is consequently increased. PL phosphors based on $\text{Y}_3\text{Al}_{5-x}\text{Ga}_x\text{O}_{12}$ garnet (YAGG, x from 0 to 5) have also been the focus of numerous studies in the last decade. In 2015, Tanabe's group developed YAGG: Cr^{3+} phosphors showing deep red PL. The persistent radiance of the optimized composition ($\text{Y}_3\text{Al}_{5-x}\text{Ga}_x\text{O}_{12}:\text{Cr}^{3+}$ where $x = 3$) was even higher than that of the $\text{ZnGa}_2\text{O}_4:\text{Cr}^{3+}$ persistent phosphor, which makes this phosphor an ideal candidate for bioimaging.⁸ The same research group also demonstrated that $\text{Y}_3\text{Al}_2\text{Ga}_3\text{O}_{12}:\text{Ce}^{3+}, \text{Cr}^{3+}, \text{Nd}^{3+}$ phosphor showed near-infrared (NIR) long PL at multi-wavelengths of around 880, 1064, and 1335 nm after excitation with blue light thanks to the efficient energy transfer (ET) from Ce^{3+} to Nd^{3+} in garnet hosts, Cr^{3+} ions acting as electron trapping.⁹ The intense NIR PL bands from Nd^{3+} match well with the first and also with the second biological window (1000–1400 nm), where radiation presents deeper tissue penetration and produces lower autofluorescence, thus resulting in higher spatial and temporal bioimages compared to the first window.¹⁰

It is well established that the use of probes for biological applications requires nanoparticulated materials with uniform

^aInstituto de Ciencia de Materiales de Sevilla (CSIC-Universidad de Sevilla), c/Américo Vespucio, 49, 41092 Sevilla, Spain. E-mail: anieto@icmse.csic.es; Tel: +34 9544489545

^bInstituto de Ciencia de Materiales de Aragón (CSIC-Universidad de Zaragoza) and CIBER-BBN, Edificio I+D, c/Mariano Esquillor s/n, 50018 Zaragoza, Spain

† Electronic supplementary information (ESI) available. See DOI: <https://doi.org/10.1039/d2qi00480a>



shape and appropriate size (<200 nm).¹¹ Moreover, nanoparticles (NPs) should be colloidally stable in physiological media and present no toxicity, the latter being especially important for *in vivo* assays.¹² Despite the interesting PL properties of YAGG-based phosphors, which exceed the performance of most other persistent phosphors, it is surprising that the development of synthesis methods to fabricate uniform YAGG micro and nanoparticles is not mature at all. YAGG-based PL phosphors were fabricated by the authors cited above by solid-state reaction at 1600 °C, which produces highly sintered material. Other synthesis methods like the Pechini sol-gel,^{13,14} modified Pechini sol-gel,¹⁵ and coprecipitation,¹⁶ followed by calcination at high temperature, were also employed to synthesize YAGG-based PL phosphors. All these methods led to ceramic materials with uncontrolled shape and size, not useful for the aforementioned bio-applications. The only synthesis method with a certain control over particles growth was that reported by Wu *et al.*,¹⁷ consisting of a salt microemulsion method. The method rendered irregular YAGG nanoparticles with an average size of 92 nm and hydrodynamic diameter of 255 nm, which indicated that the NPs were aggregated in water. It is highly desirable, therefore, to exploit new methods for the synthesis of colloidally stable YAGG-based nanoparticles with controlled shape and size and long NIR PL, and absence of toxicity, which can substantially promote their application in bioimaging.

In this study, we describe the synthesis of highly uniform $\text{Y}_3\text{Al}_2\text{Ga}_3\text{O}_{12}:\text{Ce}^{3+}, \text{Cr}^{3+}, \text{Nd}^{3+}$ nanophosphors through solvothermal reaction in polyol medium at 225 °C. The reaction rendered perfect nanospheres that were subsequently covered with a silica shell and calcined at high temperature to improve their luminescence properties. After silica removal, the NPs were functionalized with poly(acrylic acid) (PAA), and their colloidal stability was thoroughly evaluated in different physiological media. The luminescence properties of the resulting $\text{Y}_3\text{Al}_2\text{Ga}_3\text{O}_{12}:\text{Ce}^{3+}, \text{Cr}^{3+}, \text{Nd}^{3+}$ NPs were analyzed in terms of excitation and emission spectra and PL decay curves of the visible and NIR emissions. Finally, cytotoxicity was thoroughly assessed in MIA PaCa-2 cell line by MTT ((3-(4,5-dimethylthiazol-2-yl)-2,5-diphenyltetrazolium bromide) assay to evaluate the applicability of YAGG-based NPs as PL bioprobes. This is, to the best of our knowledge, the first time that colloidal YAGG-based nanoparticles are reported in the literature.

2. Experimental

2.1. Materials

2.1.1. Chemicals. Chemicals used for particles synthesis: yttrium(III) acetate hydrate ($(\text{CH}_3\text{CO}_2)_3\text{Y}\cdot x\text{H}_2\text{O}$, Sigma Aldrich, 99.9%), aluminum isopropoxide ($\text{Al}[\text{OCH}(\text{CH}_3)_2]_3$, Sigma ≥98%), aluminum acetylacetonate ($\text{C}_{15}\text{H}_{21}\text{AlO}_6$, Sigma Aldrich, 99.99%), gallium(III) acetylacetonate ($\text{C}_{15}\text{H}_{21}\text{GaO}_6$, Sigma Aldrich, 99.99%), gallium(III) nitrate hydrate ($\text{Ga}(\text{NO}_3)_3\cdot x\text{H}_2\text{O}$, Sigma Aldrich 99.9%), cerium(III) acetate hydrate ($(\text{CH}_3\text{CO}_2)_3\text{Ce}\cdot x\text{H}_2\text{O}$, Sigma Aldrich, 99.99%), chromium(III)

acetate hydroxide ($(\text{CH}_3\text{CO}_2)_7\text{Cr}_3(\text{OH})_2$, Sigma Aldrich), neodymium(III) acetate hydrate ($(\text{CH}_3\text{CO}_2)_3\text{Nd}\cdot x\text{H}_2\text{O}$, Sigma Aldrich, 99.9%), 1,4-butanediol (BG, Sigma Aldrich, 99%), diethylene glycol (DEG, Sigma Aldrich, 99%), ethylene glycol (EG, Sigma Aldrich, 99.8%), glycerol (Gly, Sigma Aldrich, ≥99.5%).

Chemicals used for silica coating: ethanol absolute for analysis (Emsure), ammonia (NH_3 , Panreac, 30%), TEOS (30% tetraethyl orthosilicate ($\text{C}_8\text{H}_{20}\text{O}_4\text{Si}$, Sigma Aldrich), hydrochloric acid (HCl, Panreac, 37%).

Chemicals used for particles functionalization and study of colloidal stability: poly(acrylic acid) (PAA, average $M_w \sim 1800$, Sigma Aldrich), 2-(*N*-morpholino)ethanesulfonic acid (MES, $\text{C}_6\text{H}_{13}\text{NO}_4\cdot \text{S}\cdot \text{H}_2\text{O}$, Sigma Aldrich, ≥99%), phosphate-buffered saline (PBS, Sigma Aldrich), physiological saline solution (NaCl-0.9%, Braun), sodium hydroxide (NaOH, ≥98%, Sigma Aldrich).

Chemicals used for cytotoxicity study: MIA-PaCa-2 cells, complete Advanced Dulbecco's Modified Eagle Medium (cDMEM; Gibco®, Thermo Fisher Scientific), fetal bovine serum (FBS, BioWhittaker™), glutaMAX™, penicillin/streptomycin (Gibco®, Thermo Fisher Scientific), Triton X-100, MTT ((3-(4,5-dimethylthiazol-2-yl)-2,5-diphenyltetrazolium bromide).

2.1.2. Synthesis of $\text{Y}_3\text{Al}_2\text{Ga}_3\text{O}_{12}:\text{Ce}^{3+}, \text{Cr}^{3+}, \text{Nd}^{3+}$ nanoparticles (AP-NPs). YAGG: $\text{Ce}^{3+}, \text{Cr}^{3+}, \text{Nd}^{3+}$ nanoparticles with nominal composition $(\text{Y}_{2.955}\text{Ce}_{0.015}\text{Nd}_{0.03})(\text{Al}_{1.999}\text{Cr}_{0.001})\text{Ga}_3\text{O}_{12}$ were fabricated following a solvothermal method. Doping concentration was taken from Xu *et al.*⁸ Yttrium acetate (7.3875×10^{-1} mmol), aluminum isopropoxide (4.9975×10^{-1} mmol), gallium acetylacetonate (7.5×10^{-1} mmol), cerium acetate (3.75×10^{-3} mmol), chromium acetate (2.5×10^{-4} mmol), and neodymium acetate (7.5×10^{-3} mmol) were dissolved in a total volume of 5 mL, mixture of BG/DEG (volumetric ratio 90/10). The suspension was stirred at 60 °C for 24 h at 400 rpm. The resultant milky solution was poured into a Teflon-lined hydrothermal reactor ($V_t = 25$ mL) and heated at 225 °C for 7 days. The white precipitate collected was washed three times with ethanol and twice with distilled water using an ultracentrifuge. The as-prepared NPs will be called AP-NPs from now on.

2.1.3. Coating AP-NPs with SiO_2 (AP-NPs@ SiO_2). To avoid aggregation during thermal treatment, the AP-NPs were coated with a silica layer following a modified Stöber method¹⁸ and optimizing the parameters of the synthesis to obtain the desired shell thickness. Briefly, the method was as follows: 5 mL of an ethanol suspension of AP-NPs (3.03 mg mL^{-1}) was prepared with help of sonication. This dispersion was poured in a Pyrex tube with the addition of distilled water (0.050 mL water per mL EtOH), NH_3 (0.150 mL NH_3 per mL EtOH), and TEOS (4.805 μL TEOS per mL EtOH). The resulting mixture was stirred at 200 rpm in a water bath at 50 °C for 1 hour. After being aged, it was washed three times with EtOH and twice with distilled water by centrifugation. The obtained suspension was dried at 60 °C. The resultant NPs will be called AP-NPs@ SiO_2 from now on.

2.1.4. Calcination of AP-NPs@ SiO_2 and removal of silica shell (C-NPs). The AP-NPs@ SiO_2 were annealed at 1000 °C in



air for 4 h at $10\text{ }^{\circ}\text{C min}^{-1}$ using an alumina well covered by another alumina well. The calcined sample (28 mg) was suspended in 0.745 mL of diluted (3%) HF and stirred at $20\text{ }^{\circ}\text{C}$ for 3 h at 300 rpm. The resulting dispersion was washed three times with distilled water by centrifugation. The resultant NPs will be called C-NPs from now on.

2.1.5. Functionalization of C-NPs (C-NPs@PAA). The NPs obtained after calcination and removal of silica shell were functionalized with PAA to improve their colloidal stability in physiological media. For this purpose, 10 mg of C-NPs were dispersed in 10 mL of Milli-Q water and the pH was increased to 10 using 1 M NaOH solution. Subsequently, 20 mg PAA were added and the pH was increased to 10 with NaOH. The resultant suspension was stirred at $20\text{ }^{\circ}\text{C}$ for 1 h at 250 rpm and the product was washed three times with distilled water by centrifugation.

2.2. Characterization techniques

2.2.1. Morphological and structural characterization. The morphology of the NPs was examined by using a transmission electron microscopy (TEM, JEOL2100Plus). The micrographs were used to estimate the mean particle size by measuring several hundreds of particles using the free software ImageJ. The hydrodynamic diameter of the NPs was measured by using a Malvern Zetasizer Nano-ZS90. A JASCO FT/IR-6200 IRT-5000 instrument was used to measure FTIR spectra of a pellet with the powdered sample diluted in KBr. A Panalytical X'Pert Pro diffractometer (CuK α) with an X-Celerator detector over an angular range of $10^{\circ} < 2\theta < 120^{\circ}$, step width of $0.05^{\circ}2\theta$ and 1 s measuring time per step, was used to examine the crystalline phase of the NPs.

2.2.2. Optical characterization. An Edinburgh FLS100 spectrofluorometer equipped with a PMT NIR detector was used to record the excitation and emission spectra of the powders in a quartz cell (20-C/Q/0.5, Starna Scientific). The same equipment was used to record Ce $^{3+}$ ($\lambda_{\text{em}} = 520\text{ nm}$) and Nd $^{3+}$ ($\lambda_{\text{em}} = 880\text{ nm}$) PL decay curves after illumination at 430 nm for 5 minutes. The excitation and emission slits were opened to maximize the intensity and a neutral density filter (OD 3) was placed in the emission pathway to avoid saturation of the detector during the excitation. The filter was quickly removed to record the PL decay curves.

2.2.3. Cytotoxicity study. The effect of C-NPs@PAA on MIA-PaCa-2 cells was studied by evaluating the cell viability by MTT. Cells were cultured at $37\text{ }^{\circ}\text{C}$ in a 5% CO $_2$ atmosphere in cDMEM supplemented with 10% FBS, 2 mM glutamaxTM, and 100 U mL $^{-1}$ of penicillin/streptomycin. Briefly, MIA-PaCa-2 cells were seeded in 96 well plates at 5000 cells per well. The cells were incubated for 48 h under cell culture standard conditions and exposed to C-NPs@PAA at different concentrations of 8, 16, 31, 62.5, 125, 250, 500, and 1000 $\mu\text{g mL}^{-1}$. 0.5% of Triton X-100 was used as a death control. Cells were further incubated for 24 h. After exposure, 10 μL of 5 mg mL $^{-1}$ MTT solution was added and incubated light-protected under culture conditions for 2 hours. Absorbance intensity at 540 nm was recorded using a MultiskanTM FC Microplate Photometer.

Untreated cells were used as the control. Viability was determined with respect to the untreated cells.

3. Results and discussion

3.1. Synthesis and characterization of Y $_3$ Al $_2$ Ga $_3$ O $_{12}$:Ce $^{3+}$, Cr $^{3+}$, Nd $^{3+}$ nanoparticles

In this study, Y $_3$ Al $_2$ Ga $_3$ O $_{12}$:Ce $^{3+}$, Cr $^{3+}$, Nd $^{3+}$ nanoparticles have been prepared by precipitation from homogeneous solutions making use of the complexing ability of polyols.¹⁰ Fig. 1 (top, a) shows TEM micrographs, taken at different magnifications, of the precipitate obtained after aging, at $225\text{ }^{\circ}\text{C}$ for 7 days, a BG/DEG (volumetric ratio 90/10) solution containing stoichiometric amounts of yttrium, cerium, neodymium, and chromium acetate, aluminum isopropoxide, and gallium acetylacetonate. The method rendered well-dispersed nanospheres

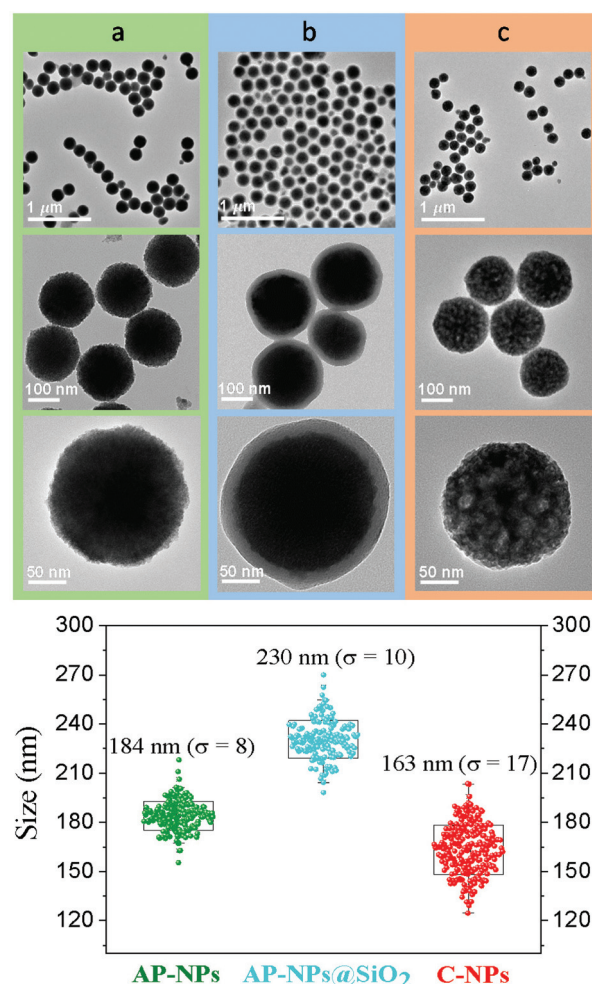


Fig. 1 Top: TEM micrographs recorded at different magnifications of (a) as-prepared NPs (AP-NPs), (b) AP-NPs covered with a silica shell (AP-NPs@SiO $_2$), and (c) AP-NPs@SiO $_2$ after calcination and HF washing (C-NPs). Bottom: Size distribution curves obtained from the TEM micrographs of the AP-NPs (green dots), AP-NPs@SiO $_2$ (blue dots), and C-NPs (red dots). σ stands for standard deviation.



(called here AP-NPs) with an average diameter of 185 ($\sigma = 8$) nm (as indicated by the histogram shown in Fig. 1 (bottom)). The nanospheres could be easily dispersed in water as shown by their hydrodynamic diameter (228 nm, Fig. S1†), which was very similar to the value measured on the TEM micrographs, indicating the practical absence of particle aggregation.

The experimental XRD pattern of the AP-NPs is shown in Fig. 2 (top). The reflections matched well with those of $\text{Y}_3\text{Al}_2\text{Ga}_3\text{O}_{12}$ reported in PDF 01-075-0556. No additional reflections were observed in the pattern, which demonstrates the purity of the reaction product. The XRD pattern was analyzed using the Rietveld method to obtain the unit cell parameters of the YAGG crystal structure. The starting structural parameters were taken from Nakatsuka *et al.*¹⁹ for undoped $\text{Y}_3\text{Al}_2\text{Ga}_3\text{O}_{12}$. The resulting calculated pattern is shown in Fig. S2,† together with the experimental one and the difference curve. It can be observed that all reflections could be successfully fitted on the basis of a cubic unit cell with space group $Ia\bar{3}d$ (230), corresponding to the crystal structure of all members in the yttrium aluminum garnet family. The cubic cell parameter of the AP-NPs was 12.196(1) Å, which is slightly

larger than that reported for undoped $\text{Y}_3\text{Al}_2\text{Ga}_3\text{O}_{12}$, (12.155 Å).¹⁹ This result can be explained as the effect of Ce^{3+} and Nd^{3+} dopants, replacing smaller Y^{3+} , on the unit cell size.

The experimental conditions described above for the synthesis of uniform $\text{Y}_3\text{Al}_2\text{Ga}_3\text{O}_{12}:\text{Ce}^{3+},\text{Cr}^{3+},\text{Nd}^{3+}$ NPs were found to be very restrictive, as the change of any of them, keeping the rest constant, did not result in the precipitation of small, uniform particles as those in Fig. 1. For example, the use of gallium isopropoxide or gallium nitrate instead of gallium acetylacetonate resulted in heterogeneous, aggregated nanoparticles (Fig. S3a and b,† respectively). Likewise, the use of aluminum acetylacetonate instead of aluminum isopropoxide did not render uniform particles (Fig. S3c†). The nature of the polyols used as solvent had also a drastic influence on the morphology of the precipitate. Specifically, the use of EG or glycerol instead of DEG in the BG/DEG mixture gave rise to the precipitation of heterogeneous particles (Fig. S3d†) and an amorphous precipitate (Fig. S3e†), respectively. The BG/DEG ratio determined the NPs size so that both higher and lower BG/DEG ratios (Fig. S3f and g,† respectively) gave rise to bigger NPs than those in Fig. 1. Reaction times shorter than 7 days resulted in a mixture of small NPs plus an amorphous precipitate (Fig. S3h†). The amount of the latter decreased with increasing reaction time and it fully disappeared after 7 days. The reaction temperature was found crucial to obtain uniform nanospheres, as heating at a lower temperature (170 °C) did only result in the precipitation of an ill-defined precipitate (Fig. S3i†). Finally, the use of double or half reactants concentration than those described in Fig. 1 led to, respectively, a heterogeneous precipitate (Fig. S3j†) and to spherical NPs with a broad size distribution (Fig. S3k†), respectively.

This is, to the best of our knowledge, the first time that nanoparticles of $\text{Y}_3\text{Al}_2\text{Ga}_3\text{O}_{12}:\text{Ce}^{3+},\text{Cr}^{3+},\text{Nd}^{3+}$ with a well define shape and uniform size are reported in the literature. The synthesis of uniform nanoparticles of other garnet-based structures with interesting optical properties such as $\text{Gd}_3\text{Al}_2\text{Ga}_3\text{O}_{12}$ or $\text{Y}_3\text{Sc}_2\text{Ga}_3\text{O}_{12}$ is missing in the literature, while limited examples of uniform $\text{Y}_3\text{Al}_5\text{O}_{12}$ -based NPs can be found in a recent review by Berends *et al.*²⁰

The AP-NPs were subsequently coated with a uniform silica shell using the modified Stöber method. The coating aimed to preserve the shape and size of the particles during calcination through the formation of a silica layer around the spheres that could be removed after the thermal process. The TEM micrographs in Fig. 1 (top, b) demonstrate that the method yielded a uniform shell on the NPs surface. The size of the AP-NPs increased from 185 ($\sigma = 8$) to 230 ($\sigma = 10$) nm after the coating process (Fig. 1, bottom), which corresponds to a shell thickness of 22 nm. The FTIR spectrum of the coated NPs (Fig. 2, bottom) confirms the success of the silica coating, as revealed by the strong doublet band located at 1090 cm^{-1} and 1220 cm^{-1} and a weaker band at around 948 cm^{-1} , which originate from the characteristic vibrational stretching Si–O modes and surface silanol (Si–OH) groups, respectively.²¹ The FTIR spectrum shows as well two intense bands located at low wavenumbers (795–250 cm^{-1}) that are assigned to metal–oxygen

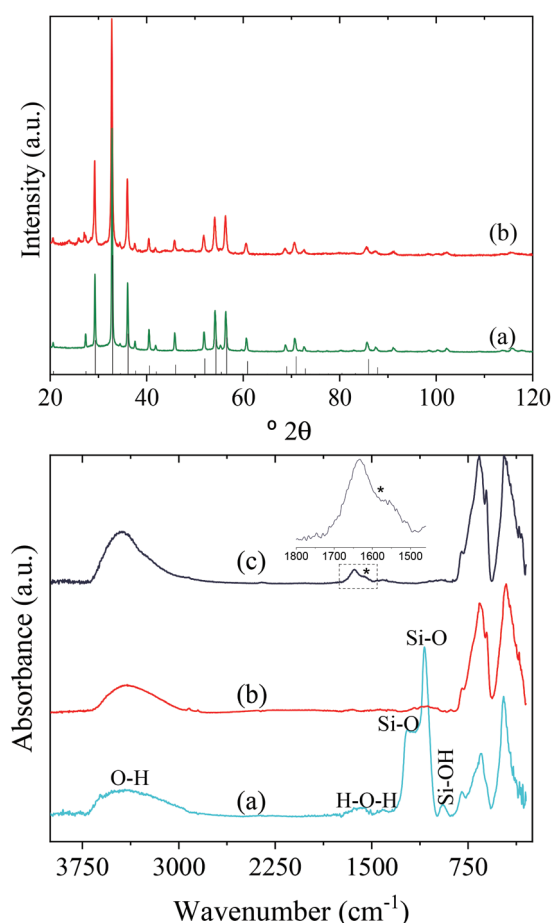


Fig. 2 Top: XRD patterns of the AP-NPs (a) and C-NPs (b) together with the reflections corresponding to $\text{Y}_3\text{Al}_2\text{Ga}_3\text{O}_{12}$ garnet (PDF 01-075-0556). Bottom: FTIR spectra of the AP-NPs@SiO₂ (a), C-NPs (b), and C-NPs@PAA (c).



vibrations of the garnet lattice²² and the characteristic stretching ($\sim 3400\text{ cm}^{-1}$) and bending ($\sim 1637\text{ cm}^{-1}$) modes of water molecules adsorbed on the NPs surface.

The AP-NPs@SiO₂ were subsequently calcined at 1000 °C in air and the calcination product was then washed with HF giving rise to highly uniform NPs (C-NPs) (Fig. 1, top, c) with an average diameter of 163 ($\sigma = 17$) nm (Fig. 1, bottom). The lower size of the C-NPs compared with the AP-NPs could be due to the shrinkage caused by the calcination process. Their hydrodynamic diameter (228 nm) (Fig. S1†), only slightly larger than the size obtained from the TEM micrographs, indicated that the C-NPs were well dispersed in water. The C-NPs showed the same crystalline phase as the AP-NPs (Fig. 2, top) and a very similar cubic cell parameter (12.205(1) Å). The characteristic bands of SiO₂ are absent in the FTIR spectrum of C-NPs (Fig. 2, bottom), which demonstrates the efficacy of HF washing to fully remove the silica coating.

3.2. Luminescent properties of Y₃Al₂Ga₃O₁₂:Ce³⁺,Cr³⁺,Nd³⁺ nanoparticles

Xu *et al.*⁹ demonstrated that Y₃Al₂Ga₃O₁₂:Ce³⁺,Cr³⁺,Nd³⁺ bulk phosphor synthesized by solid-state reaction showed near-

infrared (NIR) long PL in the NIR region due to 4f electronic transitions of Nd³⁺ ions after excitation with blue light thanks to the efficient energy transfer (ET) from Ce³⁺ to Nd³⁺ in garnet hosts, Cr³⁺ ions acting as electron trapping. The green curve in Fig. 3a corresponds to the photoluminescence emission spectrum of the AP-NPs recorded under 430 nm excitation (corresponding to the 4f–5d₂ transition in Ce³⁺ ions).²³ The spectrum showed a typical Ce³⁺:5d–4f strong broad band emission centered at 520 nm. A weak peak can also be observed at 692 nm corresponding to the emission of Cr³⁺ ions (²E → ⁴A₂). However, despite the highly efficient Ce³⁺ → Nd³⁺ energy transfer described in garnet hosts,^{8,24} no emission from Nd³⁺ could be detected in this sample. The reason behind this could be the temperature of the solvothermal method used here to synthesize the AP-NPs. This temperature, much lower than those used in classical solid-state reactions, leads to defect crystal lattices that considerably reduce the intensity of the luminescent emission.²⁵ To minimize this effect, the AP-NPs were submitted to calcination preceded by silica coating to avoid NPs aggregation, as described above. The emission spectrum of the resulting C-NPs (Fig. 3a, blue line) did clearly show, in addition to more intense Ce³⁺ and Cr³⁺ bands, several sharp

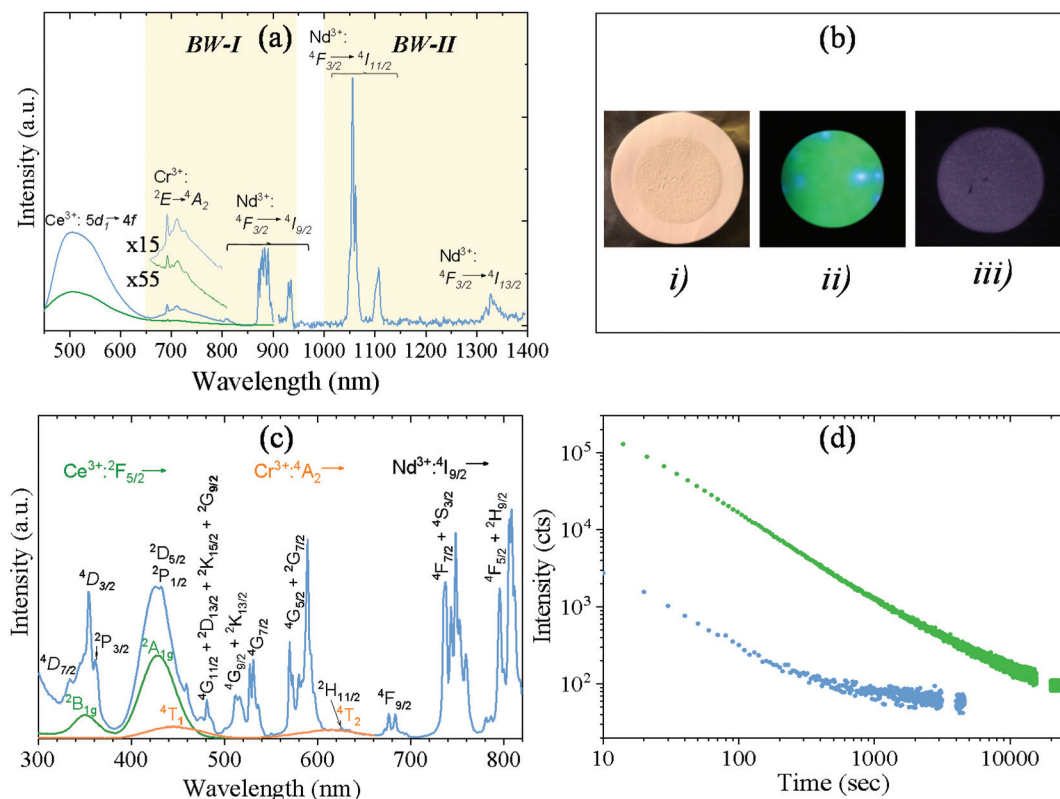


Fig. 3 (a) Emission spectra, under 430 nm excitation, of the AP-NPs (green curve) and C-NPs (blue curve). The latter was recorded using two different PMTs: a red PMT up to 900 nm and a NIR PMT from 900 nm. The insets are magnifications of the Cr³⁺ emission region for both spectra. (b) Photographs of the C-NPs sample taken while illuminating with a white LED at 8500 K (i), with a Xe lamp at 428 nm recording emission in the visible range (ii) and with a blue LED recording emission at $\lambda > 900$ nm (arbitrary color) (iii). (c) Excitation spectrum of the C-NPs monitored at the characteristic Cr³⁺ emission at 692 nm (orange curve), Ce³⁺ emission at 505 nm (green curve), and Nd³⁺ emission at 880 nm (blue curve). (d) PL decay curves of the C-NPs recorded at 520 nm (green curve) and at 880 nm (blue curve), after being illuminated with a xenon lamp at 430 nm for 5 minutes. Background counts are represented at the end of each curve.



emission bands at around 880 nm, 1063 nm, and 1335 nm, that correspond to the f-f transitions in Nd^{3+} ions, as labeled in the figure. Therefore, the C-NPs, under Ce^{3+} excitation, showed emission in the NIR region (first and second biological windows), due to Cr^{3+} and Nd^{3+} ions, as well as in the visible region, due to Ce^{3+} ions. Fig. 3b shows photographs of the C-NPs sample under natural light (i) and under blue excitation recording the visible emitted light (ii) and the emission at $\lambda > 900$ nm (iii).

The excitation spectrum of the C-NPs recorded at 520 nm (the emission wavelength characteristic of Ce^{3+} ions), is shown in Fig. 3c (green line). It shows two broad bands centered at 350 nm and 430 nm, corresponding to the transitions from the $^2\text{F}_{5/2}$ ground state to the $^2\text{B}_{1g}$ and $^2\text{A}_{1g}$ excited states, respectively, of Ce^{3+} ions.²³ The same figure (orange line) shows the excitation spectrum of the C-NPs recorded at the emission wavelength characteristic of the Cr^{3+} ion (695 nm). It shows two low-intensity broad bands at ~ 450 nm and ~ 620 nm that are assigned to the Cr^{3+} transition from $^4\text{A}_2$ to $^4\text{T}_1$ and $^4\text{T}_2$, respectively. Both Cr^{3+} and Ce^{3+} bands are observed, overlapped by several sharp excitation bands, in the excitation spectrum of the same sample, recorded while monitoring the characteristic emission of Nd^{3+} at 880 nm (Fig. 3c, blue line). The sharp bands correspond to electronic transitions from the $^4\text{I}_{9/2}$ ground state to several excited states of Nd^{3+} , as labeled in the figure. The observation of the Ce^{3+} and Cr^{3+} excitation bands while monitoring the Nd^{3+} emission is a clear evidence of the $\text{Ce}^{3+} \rightarrow \text{Nd}^{3+}$ and $\text{Cr}^{3+} \rightarrow \text{Nd}^{3+}$ energy transfer in $\text{Y}_3\text{Al}_2\text{Ga}_3\text{O}_{12}:\text{Ce}^{3+},\text{Cr}^{3+},\text{Nd}^{3+}$.^{16,26}

The persistent luminescent decay curve, monitoring the Ce^{3+} emission at 520 nm, in the C-NPs samples after being illuminated with 430 nm blue light for 5 minutes is shown in Fig. 3d (green curve). Despite the $\text{Ce}^{3+} \rightarrow \text{Nd}^{3+}$ ET, the Ce^{3+} ions still showed a strong green emission that could be detected for more than 2 hours. This long persistence of green light, to which the human eye is very sensitive, makes these nanophosphors very attractive as luminescent markers for medical use without the need for any electronic detector. In addition, the C-NPs showed persistence in the NIR region, as demonstrated by the decay curve recorded while monitoring the Nd^{3+} emission shown in Fig. 3d (blue curve). PL in the NIR region is of high interest for *in vivo* use as such radiation suffers very low absorption and scattering from blood and water, which significantly facilitates and improves light detection.

The persistent luminescence mechanism of $\text{Y}_3\text{Al}_2\text{Ga}_3\text{O}_{12}:\text{Ce}^{3+},\text{Cr}^{3+},\text{Nd}^{3+}$ phosphor was described by Xu *et al.* for the bulk material obtained through solid state reaction at 1600 °C.⁹ It consists essentially of Ce^{3+} excitation with blue light followed by jumping of the excited electron into the conduction band of the garnet and trapping by Cr^{3+} ion. The captured electron is then thermally released from the trapping center and suffers recombination with Ce^{4+} giving rise to the excited state of cerium ion (Ce^{3+*}). Cerium ion then relaxes radiatively resulting in a characteristic green emission. At the same time, energy transfer from Ce^{3+*} to Nd^{3+} takes place,

giving rise to the NIR emissions. Given that the persistent luminescence of the $\text{Y}_3\text{Al}_2\text{Ga}_3\text{O}_{12}:\text{Ce}^{3+},\text{Cr}^{3+},\text{Nd}^{3+}$ NPs fabricated here was observed after sample calcination, we think that it should follow the same mechanism as in the bulk phosphor.

3.3. Functionalization and colloidal stability in physiological media

The colloidal stability of the C-NPs was evaluated in three different buffer solutions (MES, PBS, and saline solution) to assess their suitability for biomedical applications. Fig. 4 (blue lines) shows the DLS curves obtained in all three media. The corresponding average hydrodynamic diameters (D_h) are also shown in the figure. The D_h values were, in all cases, larger than that calculated from the TEM micrographs (163 nm), especially for the PBS suspension. The DLS measurements indicated therefore that an aggregation process takes place when the NPs are suspended in the studied physiological media, the larger aggregation degree occurring in PBS. To improve the colloidal stability in physiological media, the C-NPs were functionalized with PAA. The effective coating of the C-NPs with PAA was checked by FTIR. The FTIR spectrum of the C-NPs@PAA (Fig. 2, bottom) showed, in addition to the vibrational bands observed for the nude C-NPs, an extra band at $\sim 1550\text{ cm}^{-1}$ (marked with an asterisk) that can be assigned

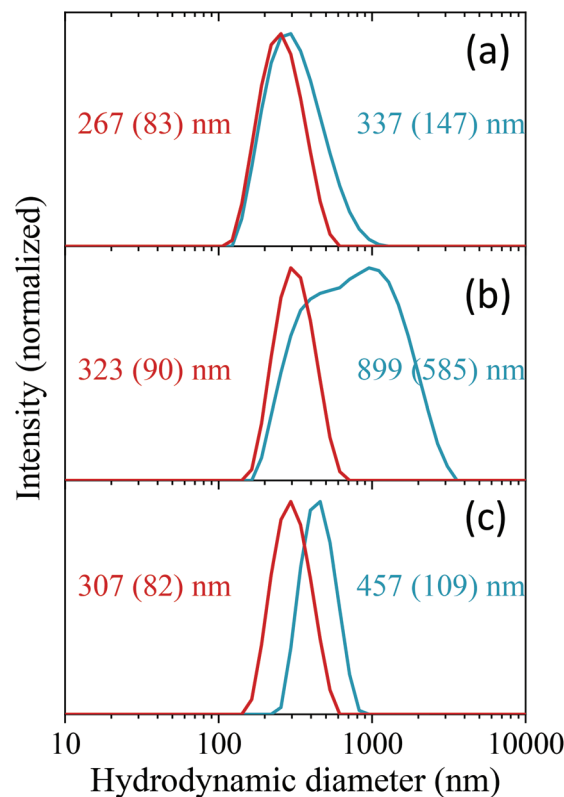


Fig. 4 DLS curves of C-NPs (blue curves) and C-NPs@PAA (red curves) suspended in MES (a), PBS (b), and saline physiological medium (c). The hydrodynamic diameters are also shown in red for the nude NPs and in black for the functionalized ones.



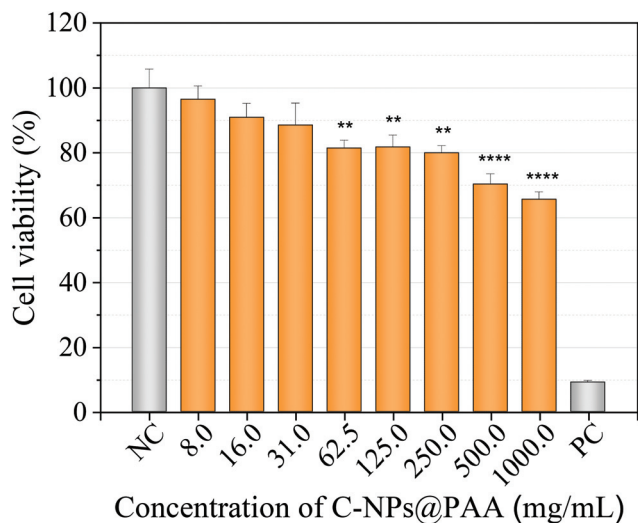


Fig. 5 Cell viability studies of MIA-PaCa-2 cell line exposed to different concentrations of C-NPs@PAA for 24 h. The results are normalized against the control (cells in DMEM, 10% FBS, considered 100%). A positive control (PC) of cell death was also included in the experimental design (0.5% Triton X-100). Data are represented as mean \pm SEM, values of $n = 3$ independent experiments are given. Statistical analysis was done by one-way ANOVA analysis followed Dunnett's multiple comparison test (** $p < 0.01$, **** $p < 0.0001$) and compared to control cell with no NPs exposure (NC).

to PAA,²⁷ which confirmed the presence of such polymer on the NPs surface.

PAA functionalization considerably improved the colloidal stability of the C-NPs, as inferred from the DLS curves, which became narrower and shifted towards lower values in all three cases, as observed in Fig. 4 (red lines). The D_h values were 267 nm, 323 nm, and 307 nm, for the MES, PBS, and saline solution suspensions, respectively, which indicate a very small degree of aggregation of the C-NPs@PAA particles in the three media.

3.4. Cytotoxicity studies

The *in vitro* cytotoxicity of the C-NPs@PAA nanoparticles was tested by MTT with the human pancreatic carcinoma cell line MIA PaCa-2 (CRL-1420™). The percentage of cell viability slightly decreased with increasing NPs concentration but, the most remarkable is that it remained above 70% for the assay with 0.5 mg mL⁻¹ of NPs (Fig. 5). These preliminary results revealed the great biocompatibility of the nanospheres exhibiting minimal cytotoxicity at the highest concentrations.

4. Conclusions

$Y_3Al_2Ga_3O_{12}:Ce^{3+},Cr^{3+},Nd^{3+}$ nanospheres have been synthesized by homogeneous precipitation in a mixture of BG and DEG (volumetric ratio 90/10) heated at 225 °C for 7 days. The experimental conditions for the synthesis of uniform NPs were found to be very restrictive, as the change of any of them,

keeping the rest constant, did not result in the precipitation of uniform NPs. The NPs obtained after the solvothermal reaction were silica-coated and calcined at 1000 °C to improve their luminescence properties. After silica removal with HF, highly uniform NPs were obtained that could be easily dispersed in water. The sample emitted green and NIR light (inside biological windows I and II) after excitation with blue light and both emissions persisted for long time after the stoppage of the excitation. The NPs could be easily functionalized with PAA and showed high colloidal stability in three different physiological media (MES, PBS, and saline solution). Likewise, the cytotoxicity studies demonstrated that the NPs were biocompatible up to, at least, 0.5 mg mL⁻¹. This study paves the way towards the use of garnet-based phosphors not only as bio-imaging probes but also for other applications that require the phosphor material to be in the form of well-dispersed nanoparticles.

Author contributions

E. Arroyo and B. Torres Herrero: investigation, formal analysis. Jesús M. de la Fuente: validation, formal analysis. Manuel Ocaña: conceptualization, supervision. Ana Isabel Becerro: methodology, writing – original draft, writing – review & editing.

Conflicts of interest

The authors declare that they have no known competing financial interests or personal relationships that could have appeared to influence the work reported in this paper.

Acknowledgements

This publication is part of the I +D+I Grants RTI2018-094426-B-I00 and PID2020-118485RB-I00 funded by MCIN/AEI/10.13039/501100011033, by “ERDF A way of making Europe”, and the Fondo Social de la DGA (grupos DGA). Financial support was also provided by Junta de Andalucía (P20_00182). Grants FPU19/00527 and FPU19/01311 were funded by MCIN/AEI/10.13039/501100011033 and by “ESF Investing in your future”. This research work was performed in the framework of the Nanomedicine CSIC HUB (Ref. 202180E048).

References

- 1 V. Castaing, E. Arroyo, A. I. Becerro, M. Ocaña, G. Lozano and H. Miguez, Persistent luminescent nanoparticles: Challenges and opportunities for a shimmering future, *J. Appl. Phys.*, 2021, **130**, 080902.
- 2 C. Chiatti, C. Fabiani and A. L. Pisello, Long Persistent Luminescence: A Road Map Toward Promising Future



- Developments in Energy and Environmental Science, *Annu. Rev. Mater. Res.*, 2021, **51**, 409–433.
- 3 S. Wu, Y. Li, W. Ding, L. Xu, Y. Ma and L. Zhang, Recent Advances of Persistent Luminescence Nanoparticles in Bioapplications, *Nano-Micro Lett.*, 2020, **12**, 70.
 - 4 A. Bessiere, S. Jacquart, K. Priolkar, A. Lecointre, B. Viana and D. Gourier, ZnGa₂O₄:Cr³⁺: a new red long-lasting phosphor with high brightness, *Opt. Express*, 2011, **19**, 10131–10137.
 - 5 A. Bessiere, S. K. Sharma, N. Basavaraju, K. R. Priolkar, L. Binet, B. Viana, A. J. J. Bos, T. Maldiney, C. Richard, D. Scherman and D. Gourier, Storage of Visible Light for Long-Lasting Phosphorescence in Chromium-Doped Zinc Gallate, *Chem. Mater.*, 2014, **26**, 1365–1373.
 - 6 M. Allix, S. Chenu, E. Veron, T. Poumeyrol, E. A. Kouadri-Boudjelthia, S. Alahrache, F. Porcher, D. Massiot and F. Fayon, Considerable Improvement of Long-Persistent Luminescence in Germanium and Tin Substituted ZnGa₂O₄, *Chem. Mater.*, 2013, **25**, 1600–1606.
 - 7 Z. Pan, V. Castaing, L. Yan, L. Zhang, C. Zhang, K. Shao, Y. Zheng, C. Duan, J. Liu, C. Richard and B. Viana, Facilitating Low-Energy Activation in the Near-Infrared Persistent Luminescent Phosphor Zn_{1+x}Ga_{2–2x}Sn_xO₄:Cr³⁺ via Crystal Field Strength Modulations, *J. Phys. Chem. C*, 2020, **124**, 8347–8358.
 - 8 J. Xu, J. Ueda, Y. Zhuang, B. Viana and S. Tanabe, Y₃Al_{5–x}Ga_xO₁₂:Cr³⁺: A novel red persistent phosphor with high brightness, *Appl. Phys. Express*, 2015, **8**, 0402602.
 - 9 J. Xu, S. Tanabe, A. D. Sontakke and J. Ueda, Near-infrared multi-wavelengths long persistent luminescence of Nd³⁺ ion through persistent energy transfer in Ce³⁺, Cr³⁺ co-doped Y₃Al₂Ga₃O₁₂ for the first and second bio-imaging windows, *Appl. Phys. Lett.*, 2015, **107**, 4.
 - 10 A. M. Smith, M. C. Mancini and S. M. Nie, Bioimaging: Second window for in vivo imaging, *Nat. Nanotechnol.*, 2009, **4**, 710–711.
 - 11 S.-K. Sun, H.-F. Wang and X.-P. Yan, Engineering Persistent Luminescence Nanoparticles for Biological Applications: From Biosensing/Bioimaging to Theranostics, *Acc. Chem. Res.*, 2018, **51**, 1131–1143.
 - 12 A. Escudero, A. I. Becerro, C. Carrillo-Carrion, N. O. Nunez, M. V. Zyuzin, M. Laguna, D. Gonzalez-Mancebo, M. Ocana and W. J. Parak, Rare earth based nanostructured materials: synthesis, functionalization, properties and bio-imaging and biosensing applications, *Nanophotonics*, 2017, **6**, 881–921.
 - 13 S. Zhang, Z. Mu, Y. Lv, L. Fan, Y. Li, G. Ju and Y. Hu, White-light long persistent luminescence of Tb³⁺-doped Y₃Al₂Ga₃O₁₂ phosphor, *J. Alloys Compd.*, 2017, **729**, 418–425.
 - 14 A. D. Lozano-Gorin, U. R. Rodriguez-Mendoza, V. Venkatramu, V. Monteseuro, M. A. Hernandez-Rodriguez, I. R. Martin and V. Lavin, Lanthanide-doped Y₃Ga₅O₁₂ garnets for nanoheating and nanothermometry in the first biological window, *Opt. Mater.*, 2018, **84**, 46–51.
 - 15 Z. Dai, V. Boiko, M. Markowska, A. Gerus, K. Grzeszkiewicz, J. Holsa, M. L. Saladino and D. Hreniak, Optical studies of Y₃(Al,Ga)₅O₁₂:Ce³⁺,Cr³⁺,Nd³⁺ nano-phosphors obtained by the Pechini method, *J. Rare Earths*, 2019, **37**, 1132–1136.
 - 16 V. Boiko, M. Markowska, L. Consentino, M. L. Saladino and D. Hreniak, Effect of Ce³⁺ concentration on persistent luminescence of YAGG:Ce³⁺,Cr³⁺,Nd³⁺ nanophosphors obtained by the co-precipitation method, *Opt. Mater.*, 2020, **107**, 109956.
 - 17 L. Y. Wu, J. Hu, Q. L. Zou, Y. L. Lin, D. C. Huang, D. J. Chen, H. Y. Lu and H. M. Zhu, Synthesis and optical properties of a Y₃(Al/Ga)₅O₁₂:Ce³⁺,Cr³⁺,Nd³⁺ persistent luminescence nanophosphor: a promising near-infrared-II nanoprobe for biological applications, *Nanoscale*, 2020, **12**, 14180–14187.
 - 18 W. Stober, A. Fink and E. Bohn, Controlled growth of monodisperse silica spheres in micron size range, *J. Colloid Interface Sci.*, 1968, **26**, 62–69.
 - 19 A. Nakatsuka, A. Yoshiasa and T. Yamanaka, Cation distribution and crystal chemistry of Y₃Al_{5–x}Ga_xO₁₂ (0 ≤ x ≤ 5) garnet solid solutions, *Acta Crystallogr., Sect. B: Struct. Sci.*, 1999, **55**, 266–272.
 - 20 A. C. Berends, M. A. van de Haar and M. R. Krames, YAG:Ce³⁺ Phosphor: From Micron-Sized Workhorse for General Lighting to a Bright Future on the Nanoscale, *Chem. Rev.*, 2020, **120**, 13461–13479.
 - 21 A. A. Ansari, S. P. Singh, N. Singh and B. D. Malhotra, Synthesis of optically active silica-coated NdF₃ core-shell nanoparticles, *Spectrochim. Acta, Part A*, 2012, **86**, 432–436.
 - 22 P. Apte, H. Burke and H. Pickup, Synthesis of yttrium-aluminum-garnet by reverse strike precipitation, *J. Mater. Res.*, 1992, **7**, 706–711.
 - 23 D. Chen, Y. Zhou, W. Xu, J. Zhong and P. Huang, Persistent and photo-stimulated luminescence in Ce³⁺/Cr³⁺ activated Y₃Al₂Ga₃O₁₂ phosphors and transparent phosphor-in-glass, *J. Mater. Chem. C*, 2016, **4**, 11457–11464.
 - 24 J. X. Meng, J. Q. Li, Z. P. Shi and K. W. Cheah, Efficient energy transfer for Ce to Nd in Nd/Ce codoped yttrium aluminum garnet, *Appl. Phys. Lett.*, 2008, **93**, 221908.
 - 25 Y. X. Pan, M. M. Wu and Q. Su, Comparative investigation on synthesis and photoluminescence of YAG : Ce phosphor, *Mater. Sci. Eng., B*, 2004, **106**, 251–256.
 - 26 P. Samuel, G. A. Kumar, T. Yanagitani, H. Yagi, K. I. Ueda and S. M. Babu, Efficient energy transfer between Ce³⁺/Cr³⁺ and Nd³⁺ ions in transparent Nd/Ce/Cr:YAG ceramics, *Opt. Mater.*, 2011, **34**, 303–307.
 - 27 E. Gomez-Gonzalez, C. Caro, D. Martinez-Gutierrez, M. L. Garcia-Martin, M. Ocana and A. I. Becerro, Holmium phosphate nanoparticles as negative contrast agents for high-field magnetic resonance imaging: Synthesis, magnetic relaxivity study and in vivo evaluation, *J. Colloid Interface Sci.*, 2021, **587**, 131–140.

